Prestressed Concrete Beam with Aramid Fibre Compression Confinement and External Tendons

HAU YIN LEUNG, City University of Hong Kong, China
CHRIS BURGOYNE, University of Cambridge, UK

INTRODUCTION

The lack of ductility of FRPs means that it is desirable for beams containing these elements as reinforcement or prestressing tendons to fail by concrete crushing, but this leads to sudden, brittle failure. It was pointed out by Burgoyne[1] that a rational approach to design was to prestress the FRP tendons, and to use confinement of the compression zone by spirals of FRP to increase the strain capacity of the concrete. The result is a beam in which the strain capacities of the tension and compression zones can be made of similar magnitude, which leads to reasonable curvatures, efficient use of the materials, and high ductility. Research at the University of Cambridge has studied the theoretical behaviour of spirally confined concrete and conducted tests on samples containing either single spirals or overlapping spirals, with forces applied either axially or eccentrically. This has led to predictions for the way a beam made in this way should behave. That work is reported in detail elsewhere[2]. This paper gives some background information and presents the final beam test that drew the various aspects of the work together.

In 1989, Mikami *et al*[3] studied the behaviour of concrete beams reinforced with FRP spirals under four-point bending. They used two different kinds of FRP, with either aramid or carbon fibres, to manufacture spiral stirrups to reinforce the compression zones of concrete beam specimens with a length of 2.25 m. They noted an improvement in both mid-span displacement and flexural strength and they also observed that the existence of spirals inside the beam influenced the crack pattern since the confined concrete hindered the propagation of flexural cracks. The use of FRP as external tendons for prestressed concrete has also been investigated[4,5]. These structures exhibit a considerable ability to accept rotation at a hinge, but this is due to large scale cracking in the tension zone and the final failure was initiated by brittle failure of the compression zone. If the strain capacity of the top fibre concrete could be increased, enhancement of beam ductility would be possible[1].

The test described here is of an 8-metre long beam prestressed with parallel-lay aramid rope tendons (Parafil) with the top flange reinforced by AFRP spirals. The beam was subjected to four-point bending; both the ductility of the top flange and the variation in tendon force were studied. Circular spirals were used since they provide a uniform distribution of confining pressure and spirals can be interlocked to allow confinement of large areas of arbitrary shape.

CHOICE OF MATERIALS

Fibres

Aramid fibres were chosen for this study. They are less brittle than carbon fibres, which aids handling in the laboratory, and for the prestressing tendons they can be used without resin.

FRPRCS-5, Thomas Telford, London, 2001.

Termination systems for the post-tensioning system are well-proven[6]. Aramids are also stiffer than glass fibres, which reduces the extension of the prestressing tendons and is important in achieving confinement. The higher modulus fibre, Kevlar 49, was used in preference to the lower modulus version. These fibres have a strength of about 2700 MPa (as yarns), with an elastic modulus of about 126 GPa.

Spirals

The composite spirals used in the compression zone of the beam were made by hand in the laboratory by taking ten yarns of fibre, dipping them in a bath of resin as they came off a creel, and then wrapping them around a collapsible mould that had a machined spiral groove of suitable depth. The resulting spiral had a diameter of 90 mm, and the pitch could be adjusted by stretching the spiral, with a consequential slight reduction in diameter.

Since it is very difficult to test the spirals directly, straight rods were made in the same way. The measured mechanical properties are given in Table 1. The relatively low conversion efficiency from the properties of the aramid fibres to the spirals is a function of the hand methods used in manufacture. Almost certainly, strengths of the order of at least 2 GPa could be achieved with mechanised fabrication, but that does not invalidate the results presented here.

Table 1. Mechanical properties of aramid spirals

Material	Cross-sectional area	Ultimate load	Ultimate stress	Ultimate strain	Elastic modulus
Kevlar 49 aramid composite (10 yarns)	1.75 mm^2 (gross) 1.13 mm^2 (fibre	2.42 kN	1.38 GPa (gross) 2.14 GPa (fibre)	1.53%	90 GPa (gross) 140 GPa (fibre)

Prestressing tendons

The Parafil rope used for the prestressing tendons is a commercial product. The rope chosen had a nominal breaking load of 600 kN, with a core area of 305.5 mm^2, and an ultimate strain of 1.77%, as measured by a tensile test using the same termination system that was used in the beams.

Concrete

There is an interaction between the stiffness of the confining spirals and the stiffness (and hence strength) of the concrete. The confinement is only induced when lateral strains occur in the concrete, and it is desirable for this to occur *before* the concrete reaches its peak strength. If the concrete is too strong, and hence too stiff, beneficial effects of confinement only become apparent after the peak load has been reached. Since the beam was being made from ready-mixed concrete, a low strength (35 MPa cube strength) was specified, but in the event the cube strengths were as high as 62 MPa at 28 days.

OUTLINE OF EXPERIMENT

To simulate practical concrete members, a T-shaped prestressed concrete beam, 8 m long, was manufactured, with an overlapping 3-D spiral network inside the top flange. Two deflected Parafil ropes were used as external tendons to provide the post-tensioning. A similar beam had been tested by Guimaraes[5] but without confinement in the compression

flange. That beam ruptured by explosive failure of the concrete in compression, and one of the objectives of the present work was to avoid that failure mechanism.

Beam details and loading arrangements

The beam cross-section is shown in Figure 1. The specimen was 0.51 m high, 0.42 m wide, and 8m long. The compression confinement was formed by interlocking six spirals in one layer. Each spiral had a diameter of 90 mm and a pitch of 35 mm, with the centre-to-centre distance between adjacent spirals of 62 mm. The beam section was splayed out to form a rectangular section at both ends to accommodate the terminals and anchorages for the tendons. The tendons were horizontal in the middle 2 m portion of the beam and then deflected upwards at an angle of 3.83° at both ends. The beam was designed so that the final failure would be initiated by rupture of the spirals after significant deformation of the compression flange. The Parafil ropes were cut to the desired lengths[7] so that the terminations were in the correct position after stressing, taking due account of initial slack and the expected behaviour of the spike and barrel anchoring system.

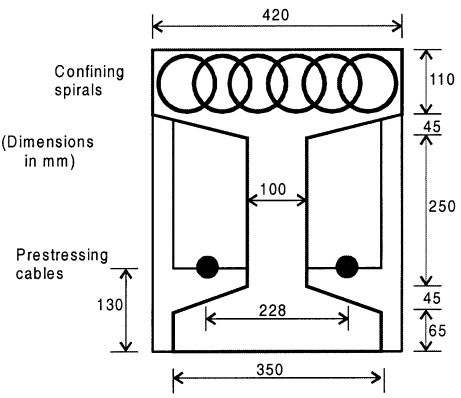

Figure 1. Beam specimen

The beam was stressed to 20% of the nominal strength of the tendons 22 days after casting, while still on the soffit shutter. This allowed the beam to be lifted onto its roller supports, which gave a clear span of 7.315 m. Five days later, the prestress was increased to 50% of the nominal strength of the tendons, which is similar to the stress that would be applied in practice taking due account of stress-rupture behaviour. The force in the tendon was monitored using load cells that were permanently installed at the dead-ends of each tendon. For security, end caps, tied back to the beam concrete, were fixed over each tendon anchorage, and external barriers were fixed at each end. Precautions were also taken against sideways movement of the beam if one tendon failed, although failure of the tendons was not expected. Four-point bending was applied from a 600 kN hydraulic jack acting through a spreader beam to give a constant moment region of 2000 mm. Various instrumentation was attached to measure strains and deflections. An overall view of the test is shown in Figure 2.

Testing procedures

The test programme was divided into three phases. In Phase I, three load cycles would be applied at 100 kN (total load), 150 kN and 200 kN. The beam was expected to crack at about 140 kN, with significant cracking at 200 kN but with the concrete in the compression zone

still elastic. In the second phase, load cycles of 220 kN and 250 kN were planned before taking the load to failure in Phase III.

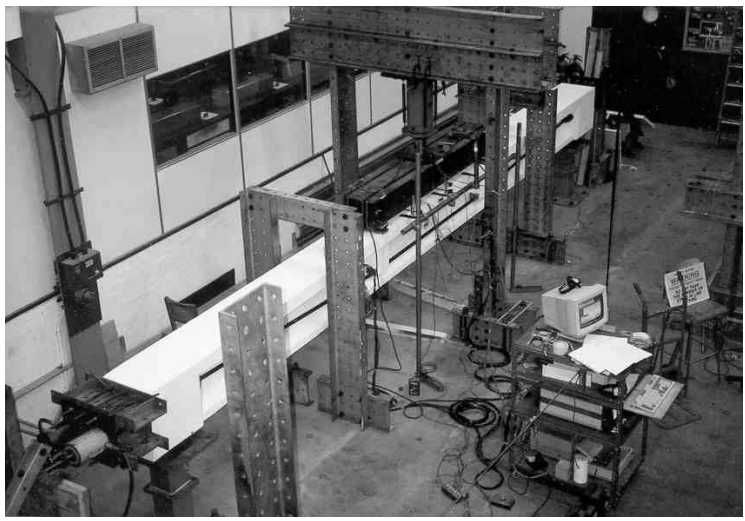

Figure 2. General view of testing setup.

ANALYTICAL FORMULATION

The flexural behaviour of a prestressed concrete member can be predicted by conventional design procedures taking the mechanical properties of FRP reinforcement into consideration. The compression zone can be divided into three regions; an unconfined region that contains the concrete outside the spirals, a singly-confined region that contains concrete inside one spiral, and a doubly-confined region that contains the concrete in the area where two spirals overlap. Stress-strain curves for the concrete in each of these areas has been derived by an extension to Kotsovos' theory[8] regarding the interaction between the hydrostatic and deviatoric components of the stresses. This theory is reported elsewhere[2] but the stress-strain curves for the different regions are shown in Figure 3. A cracked section analysis is carried out in the normal way, ignoring any concrete in tension.

Since the cables are unbonded, the forces are only transmitted from the concrete to the cables through the terminals and the deflectors, so the strain of the cable is not equal to that of the concrete at the cable level. To account for this, a bond factor, α_t, is used to determine the strain in the cable. After effective prestressing, the external unbonded cable experiences a pre-strain, which depends on the amount of applied prestress; this is denoted ε_{tp}. Under the action of bending, the concrete in the top fibre exhibits a change in strain, ε_c^o, so the strain in the concrete at the cable level (ε_{ct}) is:-

$$\varepsilon_{ct} = \left(\frac{d-x}{x} \right) \varepsilon_c^o$$

where x is the position of the neutral axis.

The strain of the cable can be calculated from :-

$$\varepsilon_t = \varepsilon_{tp} + \alpha_t \varepsilon_{ct}$$

Note that ε_c^o can go beyond the ultimate strain value of unconfined plain concrete (typically 0.0035) because of the restraining effect of the spiral confinement. The predictions for the correct value for the bond factor for steel tendons have been reported[10]; Mutsuyoshi *et al*[4] proposed a similar, but not identical, equation for FRP unbonded external cables, which implied 0.35 for α_t, obtained experimentally. In this project, 0.30 will be used after calibration using book examples[10].

Once the concrete section is divided into slices and the bond factor is assumed, the analysis can be carried out. For each value of ε_c^o, the neutral axis is varied until force equilibrium is established. The moments, curvatures and tendon force are then determined.

The change of tendon position due to overall beam deflection is taken into consideration. At each strain increment, the deflection is computed and the relative movement of tendon is incorporated in the effective depth calculations.

RESULTS AND DISCUSSIONS

Mid-span deflection

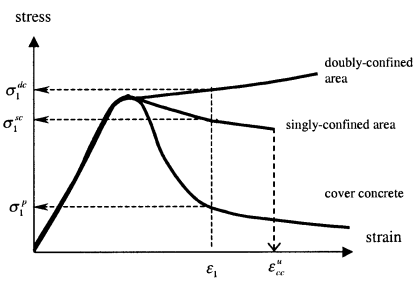

Figure 3. Stress-strain curves for different concrete layers

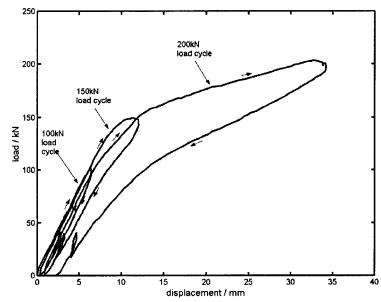

Figure 4. Phase I test: load against displacement

Figure 4 shows the response in the first phase of loading. In the first cycle, to 100 kN, the behaviour is linearly elastic. During the 150 kN load cycle, a reduction in stiffness occurs at about 140 kN, close to the expected cracking load taking account of the tensile strength of the concrete. The cracks were not visible until 150 kN when they could be observed by close inspection. A permanent deformation of 1 mm was observed from the second load cycle.

In the third cycle, the loading curve is linear until the loading approached 120 kN at which point the cracks reopened as soon as tensile stresses were induced. When loading was continued, the decrease in slope was more prominent. This indicates a further degradation in stiffness of the beam. At 200 kN, while the loading was maintained before unloading, a loud noise was heard. This was due to a bed–down of the spike in one anchorage. When the applied load was reduced to zero, an unrecoverable displacement of 2.5 mm was found. The

slope of the unloading branch decrease slightly for the second unloading and further decreased after the third cycle.

The response in the second phase of loading is shown in Figure 5, with a different scale for the displacement. The load cycle to 220 kN followed very closely the pattern of the previous load cycle, and matched closely the theory.

During the 250 kN load cycle, the response was closer to the unconfined prediction than had been expected. Significant horizontal cracking was occurring in the top flange of the beam near the centre, and at 247 kN the concrete crushed, with a significant reduction in load. On inspection it was seen that the concrete that failed was the unconfined cover concrete while the concrete in the core of the top flange remained intact.

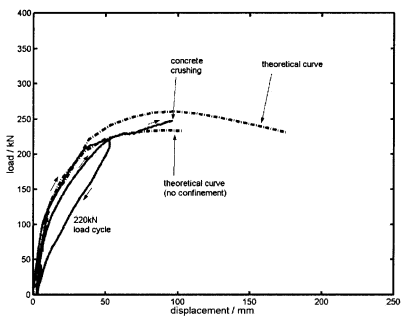

Figure 5. Phase II test: load against displacement

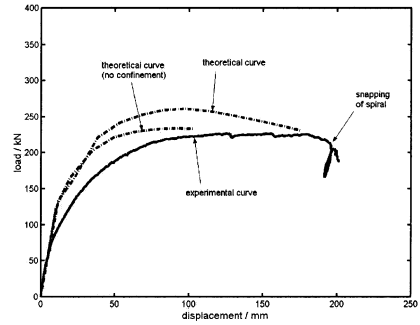

Figure 6. Phase III test: load against displacement

The results of the final loading to failure are shown in Figure 6. When the displacement reached 100 mm the beam continued to deform slowly at a virtually constant load of about 225 kN, which was less than that carried before due to the loss of concrete in the extreme compression flange. The external load was reduced slightly at 125 mm and 160 mm displacement, but the beam deformation was unchanged. When the beam had deflected by 180 mm, the sustained load started to drop slowly. The beam was deemed to have failed when the spiral snapped at a recorded displacement of 198mm.

The analytical load-deformation curves are also plotted. The theoretical model depicts the beam behaviour from the undamaged condition, with all the compression flange present. When the ascending part of the analytical model is compared with the curve in Figs 4 and 5, a close match is found.

Variation of tendon force

During the course of loading, the tendon force was monitored by means of the load cells that were located between the tendon terminations and the concrete. These results are shown in Figures 7 and 8, with one tendon referred to as Load Cell 9, and the other as Load Cell 10. For clarity, the results for Load cell 9 have been displaced by 100 kN to the right. Both tendons were carrying a force of about 290 kN before testing commenced.

For the first two load cycles the concrete strains were small so the change in length of the tendon was negligible and there was very little increase in force. For the 200 kN load cycle, significant cracks developed so the tendon force increased. The loads at which the tendon force increased match the loads at which the cracks opened, as expected.

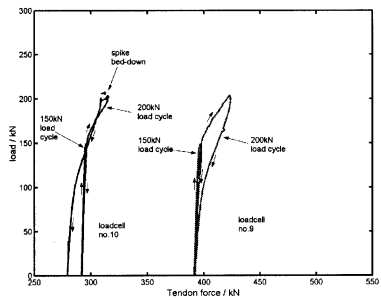

Figure 7. Phase I test: change of tendon force

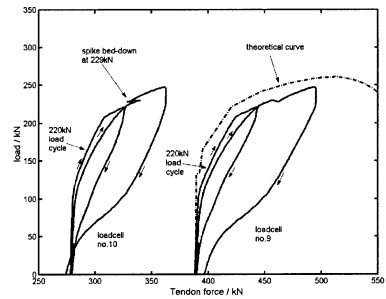

Figure 8. Phase II test: variation of tendon force

In one tendon, as indicated by load cell 10, when the load was maintained at 200 kN a noise was heard which corresponded to slip of the spike in one of the terminations. The prestress force reduced by about 15 kN. This is equivalent to a movement of the fibre of about 3mm at one end relative to the termination.

Following the ascending path of the 220 kN load-cycle (Figure 8), the tendon force remained unchanged until an external load of 100 kN was applied, when the cracks reopened. The tendon force went back to its initial value after unloading. Perfect recovery of tendon force was found for the two tendons after the first cycle despite the fact that different forces were recorded initially.

In the load cycle to 247 kN, significant beam deformations were occurring, so the tendon force increased more markedly. When the loading reached 229 kN, a second spike bed-down was recorded by load cell 10. This movement was followed by an immediate 10 kN drop in tendon force. At the same time, the other tendon experienced an equal increase, caused by redistribution of tension force to maintain equilibrium with the compression force, since the load was being maintained hydraulically. The total tendon force remained the same. The force in both tendons then increased with the applied load. The applied loading was maintained when concrete crushing occurred at the top surface, so the tendon force remained constant. During the unloading process, the tendon force reduced. It is noted that the bed-down effect at 229 kN caused a permanent change in force in both tendons. One tendon experienced a reduced force, while the other tendon increased in force.

At the beginning of the final test, the tendon forces were measured at 273 kN and 296 kN (as indicated in Figure 9, where the results for Load Cell 9 are *not* displaced). The change of tendon force in both tendons is similar. The tendon forces were kept constant when the loading was set at 225 kN. When the beam was close to failure, the load-carrying capacity reduced, due to the reduced capacity in compression, and the tendon forces decreased accordingly.

At the ultimate state, one tendon (load cell 10) was carrying a force of 414 kN, while the other (load cell 9) was carrying 451 kN. This force difference did not cause significant minor-axis bending of the specimen since the horizontal eccentricity of the tendons was small.

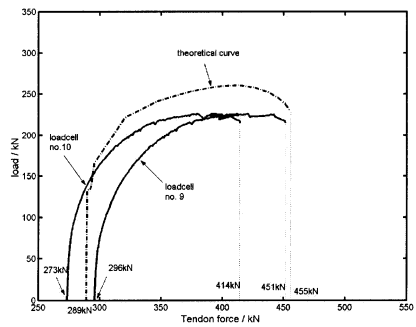

Figure 9. Phase III test: variation of tendon force (ultimate)

The analytical variation of tendon force is also shown in Figs 8 and 9. The analytical solution shows that the tendon force remains unchanged until the cracking load of 130 kN, as was observed in Fig. 7 before the section cracked. A close match of tendon force variation is indicated up to the peak load in Fig. 8. In the final test (Fig. 9) the top flange had already partly failed, so the load was lower than predicted. However, the geometrical changes, which alter the force in the tendon, still occurred, so the tendon forces at failure match the expected value reasonably well.

The final tendon force, resulting from the ultimate test, is about 70% of the ultimate strength of the tendon. In the beam tested earlier by Guimaraes[5], the final tendon force of the beam without spirals was 375 kN, which is lower than observed here. The prestressed concrete beam provided with spirals not only improves the ductility, but by allowing higher strains in the compression zone also optimises the performance of the external tendons.

Failure pattern

The crack pattern was observed and marked at load levels of 100 kN, 150 kN and 200 kN. No cracks were observed at 100 kN. Small cracks at the bottom were seen when the external load reached 150 kN. All cracks were propagating vertically. The cracks appeared only within the constant bending moment region, and all cracks were confined to the bottom flange.

At 200 kN, the crack pattern was different from that at 150 kN (Figure 10); the cracks increased in number and length. The region of cracking spread outside the middle 2 m of the beam. The cracks outside the constant moment region were mostly inclined at an angle towards the loading points, due to the shear stresses, while the cracks inside the constant bending moment region propagated upwards, as expected.

Unlike Phase I, two reductions in stiffness were observed (as indicated in Figure 5). The first was characterised by the opening of the existing flexural cracks, while the second occurred at

a higher load and related to horizontal cracking on the two sides of the top flange (Fig 11). This cracking only affected the unconfined cover concrete, outside the spirals.

During the test to failure, it was clearly observed that the cover concrete at the top flange separated from the confined concrete in the failure zone. The cracks along the bottom surface increased in size. A clear picture can be found in Figure 12.

Figure 9. Phase I test: prestressed concrete beam at 200 kN

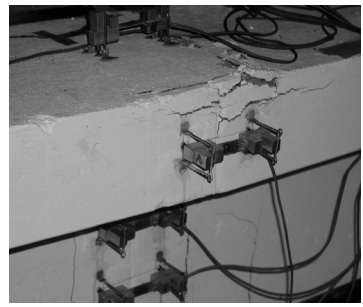

Figure 10. Phase II test: horizontal cracks

When the beam entered the region of the horizontal plateau on the load-deflection curve, horizontal cracks were observed on both sides of the top flange. Crushing of cover concrete took place gradually from the top surface. Because of the effect of the interlocking spirals, however, the confined concrete did not fail but remained effective and improved the ductility of the beam. After failure of the spiral in the compression zone, which reduced the compression force capacity, the prestress and the external load caused progressive failure in compression down the beam, finally leading to disintegration of the bottom flange (as seen in Figure 13). However, unlike the beam tested in reference 5, the failure took place gradually.

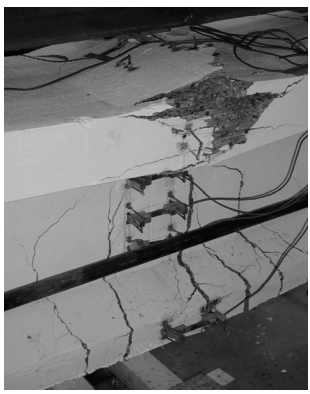

Figure 12. Phase III test: concrete section at start of final test

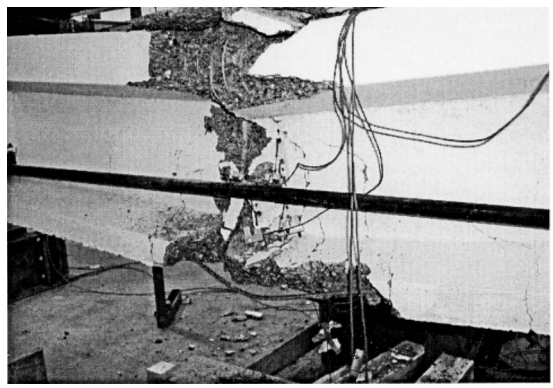

Figure 13. Phase III test: concrete section after final failure.

CONCLUSIONS

When the concrete in the compression zone of a prestressed concrete beam is confined by internally interlocked spirals, two reductions in stiffness occur at different external loads. The first, which occurs at low load values, is accompanied by flexural cracks at the bottom

flange. The second is initiated by horizontal cracking of the top flange, and happens at higher load levels.

A significant drop in load-carrying capacity was found when the cover concrete crushed at the top surface, outside the spirals. But instead of complete loss of load-carrying capacity, the beam continued to sustain loading and further deformation due to the confining action of spirals.

REFERENCES

1. Burgoyne C.J. (1997), *Rational use of Advanced Composites in Concrete*, Procs FRPRCS-3, Vol 1, 75-88.
2. Leung, H.Y. (2000) *Aramid fibre spirals to confine concrete in compression*, PhD. Thesis, University of Cambridge.
3. Mikami, H., Katoh, M., Takeuchi, H. and Tamura. T. (1989) *Flexural and Shear Behaviour of RC Beams Reinforced with Braided FRP rods in Spiral Shape*, Transaction of the Japan Concrete Institute, vol.11.
4. Mutsuyoshi, H. and Machida, A. (1993) *Behaviour of Prestressed Concrete Beams Using FRP as External Cable*, Fiber-Reinforced-Plastic Reinforcement for Concrete Structures, International Symposium, ACI, SP138-25.
5. Burgoyne, C.J., Guimaraes, G.B. and Chambers, J.J. (1991) *Tests on beams prestressed with unbonded polyaramid tendons*, Cambridge University Engineering Department Technical Report, CUED/D-Struct/TR.132.
6. Kingston D. (1988), *Development of Parallel fibre tensile members*, Procs Symposium on Engineering Applications of Parafil Ropes, 7-12, Imperial College.
7. Burgoyne, C.J. (1988) *Laboratory testing on Parafil ropes*, Symposium on Les materiaux nouveau pour la precontrainte et la renforcement d'ouvrages d'art, LCPC, Paris.
8. Kotsovos M.D. and Newman J.B., (1980) *Mathematical description of Deformational Behaviour of Concrete under Generalized Stress Beyond Ultimate Strength*, ACI Material Journal, Vol 77, Sep-Oct, 340-346.
9. Hurst, M.K. (1988) *Prestressed concrete design*, Chapman and Hall.
10. Pannell, F.N. (1969) *The ultimate moment of resistance of unbonded prestressed concrete beams*, Magazine of Concrete Research, 21, No. 66, Mar., pp.43-54.